

Search of the neutrino-less double beta decay of ^{82}Se into the excited states of ^{82}Kr with CUPID-0

O. Azzolini¹, M. T. Barrera¹, J. W. Beeman², F. Bellini^{3,4}, M. Beretta^{5,6},
M. Biassoni⁶, E. Bossio^{3,4}, C. Brofferio^{5,6}, C. Bucci⁷, L. Canonica^{7,b},
S. Capelli^{5,6}, L. Cardani^{4,a}, P. Carniti^{5,6}, N. Casali⁴, L. Cassina^{5,6},
M. Clemenza^{5,6}, O. Cremonesi⁶, A. Cruciani⁴, A. D'Addabbo^{7,8}, I. Dafinei⁴,
S. Di Domizio^{9,10}, F. Ferroni^{3,4}, L. Gironi^{5,6}, A. Giuliani^{11,12}, P. Gorla⁷,
C. Gotti^{5,6}, G. Keppel¹, M. Martinez^{3,4,c}, S. Morganti⁴, S. Nagorny^{7,8,d},
M. Nastasi^{5,6}, S. Nisi⁷, C. Nones¹³, D. Orlandi⁷, L. Pagnanini^{5,6},
M. Pallavicini^{9,10}, V. Palmieri^{1,e}, L. Pattavina^{7,8,f}, M. Pavan^{5,6}, G. Pessina⁶,
V. Pettinacci^{3,4}, S. Pirro⁷, S. Pozzi^{5,6}, E. Previtali⁶, A. Puiu^{5,6},
C. Rusconi^{7,14}, K. Schäffner⁸, C. Tomei⁴, M. Vignati⁴, A. Zolotarova¹³

¹INFN - Laboratori Nazionali di Legnaro, Legnaro (Padova) I-35020 - Italy

²Materials Science Division, Lawrence Berkeley National Laboratory, Berkeley, CA 94720 - USA

³Dipartimento di Fisica, Sapienza Università di Roma, Roma I-00185 - Italy

⁴INFN - Sezione di Roma, Roma I-00185 - Italy

⁵Dipartimento di Fisica, Università di Milano-Bicocca, Milano I-20126 - Italy

⁶INFN - Sezione di Milano Bicocca, Milano I-20126 - Italy

⁷INFN - Laboratori Nazionali del Gran Sasso, Assergi (L'Aquila) I-67010 - Italy

⁸Gran Sasso Science Institute, 67100, L'Aquila - Italy

⁹Dipartimento di Fisica, Università di Genova, Genova I-16146 - Italy

¹⁰INFN - Sezione di Genova, Genova I-16146 - Italy

¹¹CSNSM, Univ. Paris-Sud, CNRS/IN2P3, Université Paris-Saclay, 91405 Orsay, France

¹²DiSAT, Università dell'Insubria, 22100 Como, Italy

¹³CEA-Saclay, DSM/IRFU, 91191 Gif-sur-Yvette Cedex, France

¹⁴Department of Physics and Astronomy, University of South Carolina, Columbia, SC 29208 - USA

Received: date / Accepted: date

Abstract The CUPID-0 experiment searches for double beta decay using cryogenic calorimeters with double (heat and light) read-out. The detector, consisting of 24 ZnSe crystals 95% enriched in ^{82}Se and 2 natural ZnSe crystals, started data-taking in 2017 at Laboratori Nazionali del Gran Sasso. We present the search for the neutrino-less double beta decay of ^{82}Se into the 0_1^+ , 2_1^+ and 2_2^+ excited states of ^{82}Kr with an exposure of 5.74 kg·yr (2.24×10^{25} emitters·yr). We found no evidence of the decays and set the most stringent limits on the widths of these processes: $\Gamma(^{82}\text{Se} \rightarrow ^{82}\text{Kr}_{0_1^+}) < 8.55 \times 10^{-24} \text{ yr}^{-1}$, $\Gamma(^{82}\text{Se} \rightarrow ^{82}\text{Kr}_{2_1^+}) < 6.25 \times$

10^{-24} yr^{-1} , $\Gamma(^{82}\text{Se} \rightarrow ^{82}\text{Kr}_{2_2^+}) < 8.25 \times 10^{-24} \text{ yr}^{-1}$ (90% credible interval).

Keywords Double beta decay · bolometers · scintillation detector · isotope enrichment

1 Introduction

The double beta decay is a transition among isobaric isotopes $(A, Z) \rightarrow (A, Z + 2) + 2e^- + 2\bar{\nu}_e$. Despite being among the rarest processes in Nature, it was observed for eleven nuclei with typical half-lives of 10^{18} - 10^{24} years [1]. In 1937, Furry hypothesized that double beta decay could occur also without the emission of neutrinos, in the form $(A, Z) \rightarrow (A, Z + 2) + 2e^-$ [2]. This process, called neutrino-less double beta decay ($0\nu\text{DBD}$), is forbidden by the Standard Model of Particle Physics as it would violate the difference between the total number of baryons and leptons (B-L) [3,4]. Furthermore, $0\nu\text{DBD}$ is considered a golden channel to probe a fundamental property of neutrinos, i.e. their

^ae-mail: laura.cardani@roma1.infn.it

^bPresent address: Max-Planck-Institut für Physik, 80805, München, Germany

^cPresent address: Fundacion ARAID and U. Zaragoza, C/ Pedro Cerbuna 12, 50009 Zaragoza, Spain

^dPresent address: Queen's University, Kingston, K7L 3N6, Ontario, Canada

^eDeceased

^fPresent address: Physik Department, Technische Universität München, D85748 Garching, Germany

nature. This transition, indeed, can occur only if (in contrast to all the other known fermions) neutrinos coincide with their own anti-particles, as predicted by Majorana [5]. Finally, the measurement of the $0\nu\text{DBD}$ half-life would help in understanding the absolute mass scale of neutrinos, that today is one of the missing elements in the puzzle of Particle Physics [6].

CUPID-0 is the first medium-scale $0\nu\text{DBD}$ cryogenic experiment exploiting the dual read-out of heat and light for background suppression [7]. The detectors are operated as calorimeters [8]: each crystal acts as energy absorber converting energy deposits ΔE into temperature variations ΔT . The size of ΔT is determined by the crystal thermal capacitance C ($\Delta T \propto \Delta E/C$) and, for a single-particle energy deposition, it is possible to observe sizable signals only if C is extremely small. Such a small thermal capacitance is reached cooling the crystals at about 10 mK, as at cryogenic temperatures $C \propto T^3$ in accordance with the Debye law. The temperature variations are converted into readable voltage signals using a Neutron Transmutation Doped (NTD) Ge thermistor [9] glued to the crystal.

The technological effort of operating tens of massive crystals at cryogenic temperatures is motivated by the advantages that this technique offers in terms of energy resolution, efficiency, and versatility in the choice of the emitter. The CUORE experiment [10, 11, 12] is successfully operating 988 TeO_2 calorimeters for the study of the ^{130}Te $0\nu\text{DBD}$, proving the feasibility of a tonne-scale experiment based on this technology. According to the CUORE background model, the dominant contribution to the region of interest stems from α particles emitted by the materials in the proximity of the detector [13].

The primary goal of the CUPID-0 experiment is proving that the dual read-out heat/light allows to reject the α interactions, reducing the background in the region of interest for $0\nu\text{DBD}$ by an order of magnitude. This would allow to set an important milestone for next-generation projects aiming at working in an almost background-free environment to increase the discovery potential [14, 15, 16, 17]. To this purpose, each calorimeter is coupled to a light detector that enables particle identification exploiting the different light yield of different particles.

The CUPID-0 detector has been taking data since the end of March 2017 in the underground Laboratori Nazionali del Gran Sasso (LNGS) in Italy. The first data release demonstrated the potential of this technology: thanks to the strong background suppression, CUPID-0 set the most stringent limit on the half-life of the ^{82}Se decay to the ground state of ^{82}Kr [18], im-

proving by almost an order of magnitude the previous limits [19, 20] despite the small exposure.

In this work we search for the ^{82}Se decay to the 0_1^+ , 2_1^+ , 2_2^+ excited levels of its daughter, ^{82}Kr . These transitions were already studied with an exposure of 3.64×10^{24} emitters \cdot yr using a high purity Germanium detector operated underground at LNGS [21]. With an efficiency ranging from 0.3 to 3.2% (depending on the chosen signature), and a background of 9.6 ± 0.5 c/keV/y, mainly ascribed to the multi-scatter of high energy γ 's produced by close contaminations, it was possible to set the following limits on the widths of the decays: $\Gamma(^{82}\text{Se} \rightarrow ^{82}\text{Kr}_{0_1^+}) < 2.0 \times 10^{-23} \text{ yr}^{-1}$, $\Gamma(^{82}\text{Se} \rightarrow ^{82}\text{Kr}_{2_1^+}) < 5.3 \times 10^{-23} \text{ yr}^{-1}$, $\Gamma(^{82}\text{Se} \rightarrow ^{82}\text{Kr}_{2_2^+}) < 6.7 \times 10^{-23} \text{ yr}^{-1}$. In contrast to the measurements made with γ spectroscopy, in CUPID-0 we can distinguish the decay with two neutrinos emission from neutrino-less double beta decay. In this paper we present the results obtained with first data of CUPID-0 in the search of the neutrino-less double beta decay mode.

2 The CUPID-0 Detector

After an extensive R&D on scintillating crystals based on different $0\nu\text{DBD}$ emitters [22, 23, 24, 25, 26, 27, 28, 29, 30, 31, 32, 33, 34, 35] the CUPID-0 collaboration decided to focus on ^{82}Se . The high Q-value of this isotope (2997.9 ± 0.3 keV [36]) allows to reduce the background due to the environmental radioactivity, and its relatively long half-life for the 2-neutrino decay-mode ($T_{1/2}^{2\nu} = (9.2 \pm 0.7) \times 10^{19} \text{ yr}$ [37]), prevents pile-up events in the region of interest. The rather low natural isotopic abundance of ^{82}Se (8.82% [38]) was increased via isotopic enrichment to 96.3% by the URENCO Stable Isotopes unit (Almelo, Netherlands). The obtained ^{82}Se was used to synthesize the ZnSe powder, that was later purified and doped using ZnSe(Al) with natural isotopic composition of Zn and Se, in order to enhance the light output.

The ZnSe powder was used to grow 24 cylindrical ZnSe crystals 95% enriched in ^{82}Se [39]. The detector includes also two natural ZnSe crystals, not considered for this work. Since we optimized the crystal shape in order to prevent losses of enriched material, and since we had to reduce the mass of some crystals to discard inclusions and imperfections, the ZnSe detectors feature slightly different size and mass. The total mass of the 24 Zn^{82}Se crystals amounts to 9.65 kg, but two of them are not used for the analysis presented in this paper because of their poor bolometric performance. Thus, the mass considered for the analysis is 8.74 kg (3.41×10^{25} nuclei of ^{82}Se).

The light produced by the ZnSe scintillation (a few % of the total energy released as heat) escapes the crystal and is recorded using two light detectors. The fraction of energy converted in form of light depends on the nature of the interacting particle, enabling particle identification and, ultimately, the rejection of the α background [40]. In CUPID-0 also the light detectors are operated as cryogenic calorimeters, meaning that they convert the impinging photons in temperature variations using NTD Ge thermistors [41]. Nevertheless, in this paper we do not describe the details of the light detectors, as the analysis of coincidences among detectors already provides a sufficient background suppression.

The ZnSe crystals, surrounded by a VIKUITI multi-layer reflecting foil produced by 3M, and interleaved by light detectors, are assembled in 5 towers using PTFE pieces and a mechanical structure made of NOSV copper (produced by Aurubis AG). Each detector was equipped with a Si Joule resistor that periodically injects a reference pulse to correct thermal drifts [42, 43].

More details concerning the detector construction and operation, the $^3\text{He}/^4\text{He}$ dilution refrigerator, the electronics and data-acquisition can be found in Ref [7].

3 Expected Signatures in CUPID-0

The decay scheme of ^{82}Se is shown in Fig. 1.

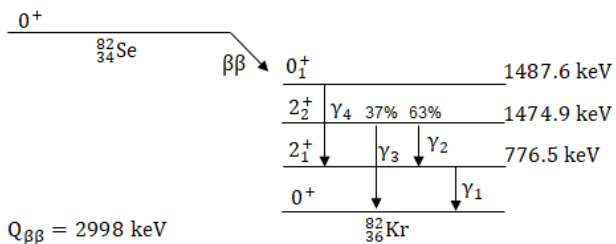


Fig. 1 Decay scheme of ^{82}Se on ^{82}Kr .

If ^{82}Se decays to the *ground* state of ^{82}Kr , the two emitted electrons share the entire Q -value of the transition. From Monte Carlo simulations, the probability for the two electrons to release the full energy in the crystal where they were emitted, thus producing a peak at the Q -value of the $0\nu\text{DBD}$, is $81.0 \pm 0.2\%$.

The scenario becomes slightly more complicated if the decay occurs to an excited level of ^{82}Kr . In this case, the energy of the decay is split between the electrons and the γ rays emitted during the de-excitation of ^{82}Kr . The containment efficiency of the two electrons does not vary significantly, but the probability that a

coincident γ ray with energy ranging from 698 keV (γ_2) to 1475 keV (γ_3) releases its full energy in the crystal is very low, leading to an important decrease of the detection efficiency. The γ rays produced in the de-excitation, indeed, can be fully absorbed in the crystal, or escape the crystal and be absorbed in another one, or escape the crystal and scatter in another crystal, or completely escape detection. Depending on the scenario, we expect different signatures. In addition, more decay schemes can result in the same signature, further complicating the analysis. The redundancy of states, as well as the different detection efficiency of the processes, impose a down-selection of the decay schemes.

First, we exclude from the analysis the events in which a *single* crystal triggers, such as those in which the γ rays escape detection. This choice is motivated by the high background produced mainly by the 2-neutrino double beta decay of ^{82}Se .

Then, we restrict the analysis to events in which *only two* ZnSe crystals trigger, thus rejecting interactions in three or more crystals. This choice, that excludes for example the scenario in which the electrons and the two γ 's interact in three different crystals, is motivated by the very low efficiency of these signatures.

Finally, we discard the remaining signatures with efficiency lower than 0.01% that would not give a substantial contribution to the analysis.

To compute the detection efficiency, we simulate 10^7 decays in the CUPID-0 crystals, accounting also for a linear smearing of the energy resolution as a function of the energy (Sec. 5). We select events in which two detectors trigger and the energy measured by one of them (E_{coinc}) is compatible with the energy of a de-excitation γ ray. Then, we search for a peak in the other crystal with energy E_{main} equal to the total energy of the two electrons $E_{\beta\beta}$, or to the sum of the energy of the electrons and another γ ray emitted in the same decay $E_{\beta\beta} + E_{\gamma_i}$. The signatures chosen for the analysis presented in this paper and their detection efficiencies are summarized in Table 1.

The number of decays N_i corresponding to the i^{th} signature can be written as a function of the exposure ($\xi = 2.24 \times 10^{25}$ emitters \times yr), the detection efficiency ϵ_i (Table 1), the data selection efficiency η (Sec. 5) and

Signature	E_{main} [keV]	E_{coinc} [keV]	ϵ [%]		
1	$\beta\beta_1 \gamma_1$	2220.5	776.5	1.817 ± 0.009	A
2	$\beta\beta_2 \gamma_1$	1522.1	776.5	0.604 ± 0.004	B
3	$\beta\beta_2 \gamma_2$	1522.1	698.4	0.664 ± 0.004	C
4	$\beta\beta_2 \gamma_3$	1522.1	1474.9	0.919 ± 0.007	D
5	$\beta\beta_2 \gamma_1 + \gamma_2$	1522.1	1474.9	0.0141 ± 0.0004	D
6	$\beta\beta_2 + \gamma_1 \gamma_2$	2298.6	698.4	0.201 ± 0.002	E
7	$\beta\beta_2 + \gamma_2 \gamma_1$	2220.5	776.5	0.211 ± 0.002	A
8	$\beta\beta_3 \gamma_2$	1509.4	776.5	0.606 ± 0.006	B
9	$\beta\beta_3 \gamma_4$	1509.4	711.1	0.660 ± 0.006	F
10	$\beta\beta_3 + \gamma_1 \gamma_4$	2285.9	711.1	0.196 ± 0.003	G
11	$\beta\beta_3 + \gamma_4 \gamma_1$	2220.5	776.5	0.200 ± 0.003	A

Table 1 Signatures of the ^{82}Se decays on the excited states of ^{82}Kr , grouped according to the decay level: $\beta\beta$ is the energy carried away by electrons in the decay to the 2_1^+ state ($\beta\beta_1$), to the 2_2^+ state ($\beta\beta_2$), or to the 0_1^+ state ($\beta\beta_3$); γ_i are the γ rays emitted in the de-excitation to the ground state (Fig. 1); the vertical bar separates the particles releasing their full energy (E_{main}) in the 1st crystal, and the particles releasing their full energy (E_{coinc}) in the second crystal. The detection efficiency ϵ is determined by a Monte Carlo simulation. Different decay schemes resulting in the same signature (for example, 1, 7, 11) are labelled with the same letter in the last column; the letter B indicates two states with a slightly different energy $\beta\beta$, that were grouped given the resolution of the detector.

the width of the corresponding decay channel (Γ):

$$\begin{aligned}
N_A &= \eta\xi \cdot [\epsilon_1\Gamma_{2_1^+} + \epsilon_7\Gamma_{2_2^+} + \epsilon_{11}\Gamma_{0_1^+}] \\
N_B &= \eta\xi \cdot [\epsilon_2\Gamma_{2_2^+} + \epsilon_8\Gamma_{0_1^+}] \\
N_C &= \eta\xi \cdot \epsilon_3\Gamma_{2_2^+} \\
N_D &= \eta\xi \cdot [\epsilon_4\Gamma_{2_2^+} + \epsilon_5\Gamma_{2_2^+}] \\
N_E &= \eta\xi \cdot \epsilon_6\Gamma_{2_2^+} \\
N_F &= \eta\xi \cdot \epsilon_9\Gamma_{0_1^+} \\
N_G &= \eta\xi \cdot \epsilon_{10}\Gamma_{0_1^+}
\end{aligned} \tag{1}$$

Each signature can be modeled with a function describing the detector response to a monochromatic energy deposit (Σ), a flat background component (ρ^{flat}) and, if the mean energy is close to the energy of the ^{40}K line (signatures B, C, D, F), a peaking background accounting for accidental coincidences due to the higher rate of this peak (Σ_{40K}):

$$\begin{aligned}
f^A &= N_A\Sigma_A + (N_A^{bkg,1} \cdot \rho_A^{flat}) \\
f^B &= N_B\Sigma_B + (N_B^{bkg,1} \cdot \rho_B^{flat} + N_B^{bkg,2} \cdot \Sigma_{40K}) \\
&\dots \\
f^F &= N_F\Sigma_F + (N_F^{bkg,1} \cdot \rho_F^{flat} + N_F^{bkg,2} \cdot \Sigma_{40K}) \\
f^G &= N_G\Sigma_G + (N_G^{bkg,1} \cdot \rho_G^{flat})
\end{aligned} \tag{2}$$

In Sec. 4 we describe how data are acquired and processed. In Sec. 5 we derive a model for the detector response Σ as a function of the energy and compute the data selection efficiency. Finally, in Sec. 6 we perform the simultaneous fit of the models $f^A \dots f^G$ to the data to extract the values of $\Gamma_{0_1^+}$, $\Gamma_{2_1^+}$ and $\Gamma_{2_2^+}$.

4 Data Collection and Processing

The temperature variation produced by 1 MeV energy deposit in a ZnSe results in a voltage signal of tens of μV , with typical rise-time of 10 ms and decay-time ranging from 15 to 60 ms, depending on the detector. The voltage signals are amplified and filtered using a Bessel 6 poles anti-aliasing filter with tunable cut-off frequency and gain (more details about the electronics and read-out can be found in Refs [44, 45, 46, 47, 48, 49, 50, 51, 52]).

The entire data-stream is digitized with a frequency of 1 kHz and saved on disk in NTuples based on the ROOT software framework. The flags of a software derivative trigger continuously running on the data are also stored in the NTuples for the off-line analysis [53, 54].

The analysis presented in this work comprises 6 DataSets, each consisting of a collection of physics runs of about 2 days, plus an initial and final calibration with ^{232}Th sources to monitor the detector stability (see Table 2). The first DataSet was devoted to the detector commissioning and optimization, and for this reason it shows the lowest fraction of live-time. This DataSet was not used for the $0\nu\text{DBD}$ analysis presented in Ref [18] because of the poor rejection of the α background due to the variations of the working conditions of the light detectors. The capability of rejecting α particles is not necessary for the analysis presented in this paper, mainly because the reflecting foil and the light detectors shield the crystals and prevent α particles from interacting in more than one detector, mimicking the searched signals. Thus, we decided to include also the first DataSet to increase the statistics.

Since the Q-value of the ^{82}Se $0\nu\text{DBD}$ to the ground state exceeds the highest γ ray produced by the ^{232}Th source (~ 2.6 MeV), after the last DataSet we made a calibration with a short-living ^{56}Co source, producing γ peaks up to 3.5 MeV. This calibration is used also to study the energy dependency of the energy resolution (Sec. 5).

The total ZnSe collected exposure (enriched crystals only) amounts to 5.74 kg·yr, corresponding to 3.05 kg·yr of ^{82}Se (2.24×10^{25} emitters·yr). These values account for the dead-time due to detector problems (such as earthquakes or major underground activities) and also

Table 2 Fraction of time that was spent in physics runs, ^{232}Th , ^{56}Co and Am-Be calibrations (Calib.) and for tests, liquid helium refills of the cryostat, software debug, DAQ problems (Other). In the last column we report the ^{82}Se exposure (enriched crystals only) collected in each DataSet.

	Physics [%]	Calib. [%]	Other [%]	Exposure [emitters·yr]
DataSet 1	60.6	16.8	22.6	3.33×10^{24}
DataSet 2	65.0	27.6	7.4	2.36×10^{24}
DataSet 3	78.6	14.1	7.3	3.68×10^{24}
DataSet 4	83.5	14.1	2.4	3.19×10^{24}
DataSet 5	82.8	11.4	5.8	4.20×10^{24}
DataSet 6	81.8	13.1	5.1	5.65×10^{24}

for the loss of two enriched crystals due to a non-satisfactory bolometric performance.

The collected data are processed off-line using a C++ based analysis framework originally developed by the CUORE-0 collaboration [55, 56, 57, 58].

The continuous data stream is converted into acquisition windows of 4 s, with a pre-trigger window of 1 second to evaluate the detector instantaneous temperature before the pulse occurred.

The data are filtered with a software matched-filter algorithm [59, 60] to improve the signal-to-noise ratio. The filtered amplitude is then corrected for gain instabilities using the reference pulses periodically injected through the Si resistors [61, 62]. The corrected amplitude is converted into energy by fitting with a parabolic function with zero intercept the most intense γ peaks produced by the ^{232}Th source between 511 keV and 2615 keV. Finally, we compute time coincidences between detectors with a coincidence window of 20 ms, earlier optimized by studying the time-distribution of real coincidence events collected during the ^{232}Th calibrations. This choice was made conservatively to ensure a 100% selection efficiency, at the cost of a possibly larger background due to accidental coincidences. Nevertheless, in the next section we show that, given the low detector rate in physics runs, the number of random coincidences is almost negligible.

5 Data Analysis

To infer the detector response to a monochromatic energy release Σ , we study the 2615 keV line produced by the decay of ^{208}Tl . As explained in Ref. [18], the simplest model describing this peak is the sum of two Gaussian functions G with two different σ and mean values: $\Sigma(\mu_1, \mu_2, \sigma_1, \sigma_2, f_{1,2}) = f_{1,2}G(\mu_1, \sigma_1) + (1-f_{1,2})G(\mu_2, \sigma_2)$.

As of today, we do not know the underlying physics behind this bi-Gaussian response. Nevertheless, a multi-Gaussian description of the signal was already observed in other experiments based on cryogenic calorimeters [55, 63]. To account for possible time-variations of the detector response, we fit this model to the 2615 keV peak in the sum energy spectrum of all the periodical ^{232}Th calibrations, obtaining $f_{1,2} = 0.83 \pm 0.03$, $\mu_1 = 2613.88 \pm 0.13$ keV, $\sigma_1 = 8.89 \pm 0.12$ keV, and $\mu_2 = 2628.37 \pm 1.42$ keV, $\sigma_2 = 15.42 \pm 0.49$ keV.

To validate the calibration with ^{232}Th sources and characterize the detector response over the range of interest, we perform a run with ^{56}Co sources, emitting many γ rays from 511 to 3451 keV. We energy-calibrated the ^{56}Co spectra with the coefficients derived from the ^{232}Th calibration, and we fit the model $\Sigma(\mu_1, \mu_2, \sigma_1, \sigma_2, f_{1,2})$ to the most prominent peaks by fixing the value of $f_{1,2}$ and the ratios μ_2/μ_1 and σ_2/σ_1 to those obtained fitting the 2615 keV line. This choice allows to fix the shape of the fit function and keep as free parameters only μ_1 and σ_1 : $\Sigma(\mu_1, \mu_2, \sigma_1, \sigma_2, f_{1,2}) \rightarrow \Sigma(\mu_1, \sigma_1)$.

The parameters μ_1 and σ_1 extracted from the fit of the most prominent ^{56}Co peaks are reported as a function of the energy in Fig. 2.

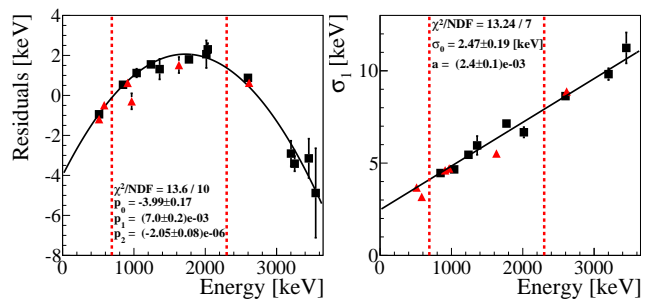


Fig. 2 Validation of the ^{232}Th calibration (red triangles) with a ^{56}Co source (black squares). All the energy spectra were calibrated using the coefficients derived from the fit of the most prominent ^{232}Th peaks. Left: residuals of the calibration, defined as (nominal energy - μ_1), as a function of the energy; the data obtained with ^{56}Co are modeled with a parabolic function (black line). Right: σ_1 as a function of the energy, modeled with a linear function (black line). The vertical dashed lines indicate the region of interest.

This study shows that the residuals of the calibration in the region of interest range from -0.5 to 2.5 keV. We check possible differences in the physics runs with respect to calibration runs by fitting the same model to the γ line of ^{40}K , obtaining $\mu_1 = 1458.11 \pm 0.41$ keV, i.e., a residual of 2.7 keV that will be treated as source of systematic error. Fig. 2 shows also that the resolution of the peaks scales linearly with the energy:

$\sigma_1(E) = \sigma_0 + aE$, with $\sigma_0 = 2.47 \pm 0.19$ keV and $a = (2.4 \pm 0.1) \times 10^{-3}$. This dependency is used to derive the correct signal model at the energy of each signature: $\Sigma(\mu_1, \sigma_1(E))$. Even if the following we will always use the bi-gaussian model, for simplicity we will drop the subscript 1 and write σ and $\Sigma(\mu, \sigma(E))$.

After deriving the signal models, we produce the energy spectra corresponding to the signatures and compute the data selection efficiency. This parameter comprises the trigger efficiency, the energy reconstruction efficiency, and the efficiency of the quality-cuts applied to the data. The trigger efficiency, computed on the reference pulses injected by the Si resistor, is defined as the ratio of the triggered to injected pulses. The energy reconstruction efficiency is defined as the number of reference pulses reconstructed within $\pm 3\sigma$ off the mean energy. Their combined value results $99.50 \pm 0.02\%$.

The data used for this analysis are selected by imposing a time-coincidence between two crystals in a 20 ms time-window. Given the low rate in physics run (~ 2 mHz) and the narrow time-window for coincidences, we expect a coincidence rate of 3.2×10^{-7} events/s in the range from 0 to 10 MeV. Adding also the requirement on the energy of the events (Table 1) brings the rate of accidental coincidences to a negligible value ranging from < 0.08 counts (signatures A, E, G) to 0.5 counts (signature B). As a consequence, there is no need to exploit the algorithms for background suppression developed for the search of the $0\nu\text{DBD}$ to the ground state [64].

On the contrary, we apply only a basic cut to the events, selecting windows in which a single pulse is present, to prevent a wrong estimation of the pulse amplitude due to an unpredictable response of the matched filter in presence of more pulses. The efficiency of this cut is computed on the most intense γ peak of the physics spectrum, due to the decay of ^{65}Zn ($T_{1/2} \sim 224$ d, $Q\text{-value} \sim 1351.9$ keV). The accepted and rejected events are simultaneously fitted with an un-binned extended maximum likelihood fit (with the RooFit analysis framework), resulting in a selection efficiency of $96.0 \pm 0.4\%$ (Fig. 3). The analysis was repeated on the γ peak produced by ^{40}K at 1.46 MeV, obtaining a compatible result ($96.0 \pm 1.1\%$). The combination of the selection efficiency with the trigger and energy reconstruction efficiencies results in a total efficiency $\eta = 95.5 \pm 0.4\%$.

6 Results

The energy spectra of signatures A, \dots , G are reconstructed starting from the selected events. Following Table 1, for each spectrum we consider a ~ 400 keV

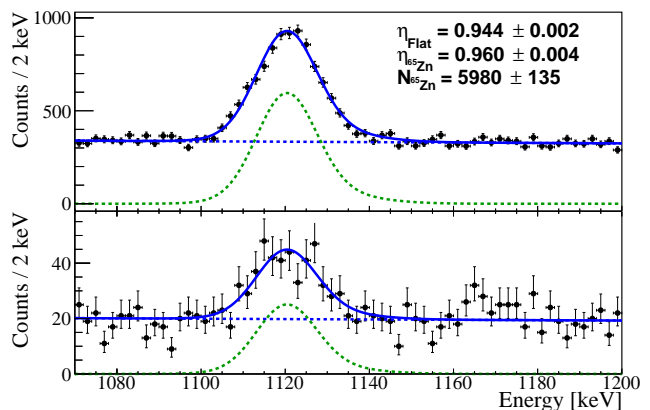


Fig. 3 γ peak produced by the decay of ^{65}Zn . Top: events in which the acquisition window contains a single pulse. Bottom: events in which the acquisition window contains more than one pulse. The spectra are fitted simultaneously with an unbinned extended maximum likelihood fit (RooFit analysis framework) with two components: the function modeling the detector response $\Sigma(\mu, \sigma(E))$, and an exponential background.

range centered around E_{main} , as this is a reasonable interval in which the background rate can be considered flat. This spectrum is further selected requiring that the events are in a 20 ms time-coincidence with events in $[E_{coinc} - 2\sigma, E_{coinc} + 2\sigma]$. The values of σ are chosen consistently with the results shown in Fig. 2.

We report in Fig. 4 the energy spectra corresponding to signatures A (< 0.08 background counts expected) and B (0.5 background counts expected), to show the two limit cases. Because of the low background rate, the spectra of the other signatures are very similar to those displayed in these plots.

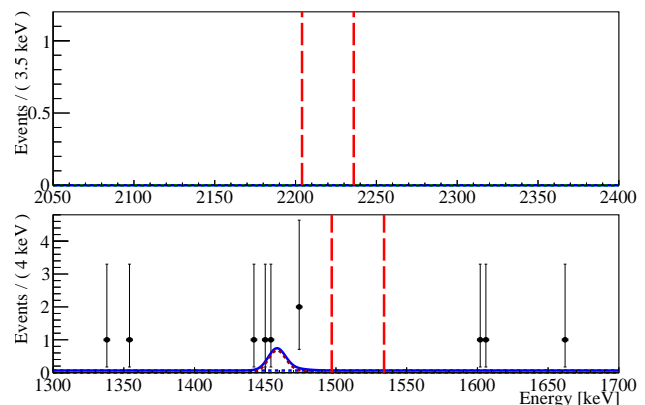


Fig. 4 Energy spectra of E_{main} corresponding to signatures A (top) and B (bottom) with an exposure of 2.24×10^{25} emitters-yr. The red vertical bars indicate a $\pm 2\sigma$ window centered around E_{main} (Table 1). The best fit result is shown in blue. A peaking background at the energy of ^{40}K , in addition to the flat background, can be observed in the bottom panel.

The decay widths are measured using a simultaneous unbinned extended maximum likelihood fit with the following free parameters: $\Gamma_{0_1^+}$, $\Gamma_{2_1^+}$ and $\Gamma_{2_2^+}$, common to all the signatures, $N_A^{bkg,1} \dots N_G^{bkg,1}$ (the number of events ascribed to the flat background in each spectrum), $N_B^{bkg,2}$, $N_C^{bkg,2}$, $N_D^{bkg,2}$ and $N_F^{bkg,2}$ (the number of events ascribed to the ^{40}K peaking background). The best fit model, reported in Fig. 4 for signatures A and B, shows no evidence of decays.

The fit accounts also for various sources of systematic errors. We evaluate the uncertainty related to the calibration function assuming an uniform distribution in the interval $[\mu-\Delta, \mu+\Delta]$, with $\Delta = 2.7$ keV, conservatively chosen from the study of the residuals.

The error due to the extrapolation of σ at the energies where we expect the decays, as well as the systematic error induced by the uncertainty on the selection efficiency η , are modeled by weighting the likelihood by a gaussian function with mean fixed to σ (η) and RMS fixed to the uncertainty on σ (η). We finally integrate the likelihood by numerical method.

The 90% credible intervals Bayesian upper limit are set using a uniform prior on the values of $\Gamma_{0_1^+}$, $\Gamma_{2_1^+}$ and $\Gamma_{2_2^+}$ and marginalizing over the flat and peaking background parameters, obtaining:

$$\begin{aligned} \Gamma(^{82}\text{Se} \rightarrow ^{82}\text{Kr}_{0_1^+}) &< 8.55 \times 10^{-24} \text{ yr}^{-1} \\ \Gamma(^{82}\text{Se} \rightarrow ^{82}\text{Kr}_{2_1^+}) &< 6.25 \times 10^{-24} \text{ yr}^{-1} \\ \Gamma(^{82}\text{Se} \rightarrow ^{82}\text{Kr}_{2_2^+}) &< 8.25 \times 10^{-24} \text{ yr}^{-1}. \end{aligned} \quad (3)$$

7 Conclusions

In this paper we presented the first background-free search of the neutrino-less double beta decay of ^{82}Se to the excited states of ^{82}Kr with an exposure of 2.24×10^{25} emitters.yr. Despite the low efficiency, we were able to set the most competitive upper limits on the decay widths of the 0_1^+ , 2_1^+ and 2_2^+ levels. The detector is still taking data at LNGS with the aim of reaching a ZnSe exposure of 10 kg.yr, that will allow to further improve this result.

Acknowledgements This work was partially supported by the Low-background Underground Cryogenic Installation For Elusive Rates (LUCIFER) experiment, funded by ERC under the European Union's Seventh Framework Programme (FP7/2007-2013)/ERC grant agreement n. 247115, funded within the ASPERA 2nd Common Call for R&D Activities. We thank M. Iannone for his help in all the stages of the detector assembly, A. Pelosi for constructing the assembly line, M. Guetti for the assistance in the cryogenic operations, R. Gaigher for the mechanics of the calibration system, M. Lindozzi for the cryostat monitoring system, M. Perego

for his invaluable help in many tasks, the mechanical workshop of LNGS (E. Tatananni, A. Rotilio, A. Corsi, and B. Romualdi) for the continuous help in the overall set-up design. A. S. Zolotorova is supported by the Initiative Doctorale Interdisciplinaire 2015 project funded by the Initiatives d'excellence Paris-Saclay, ANR-11-IDEX-0003-0. We acknowledge the Dark Side Collaboration for the use of the low-radon clean room. This work makes use of the DIANA data analysis and APOLLO data acquisition software which has been developed by the CUORICINO, CUORE, LUCIFER and CUPID-0 collaborations.

References

1. A. S. Barabash, Nucl. Phys. A **935**, 52 (2015). DOI doi.org/10.1016/j.nuclphysa.2015.01.001
2. W. H. Furry, Phys. Rev. **56**, 1184 (1939).
3. S. Dell'Oro, S. Marcocci, M. Viel, F. Vissani, Adv. High Energy Phys. **2016**, 2162659 (2016). DOI 10.1155/2016/2162659.
4. F. Feruglio, A. Strumia and F. Vissani, Nucl. Phys. B **637**, 345 (2002) Addendum: [Nucl. Phys. B **659**, 359 (2003)]. DOI 10.1016/S0550-3213(02)00345-0, 10.1016/S0550-3213(03)00228-1.
5. J. Schechter and J. W. F. Valle, Phys. Rev. D **25**, 2951 (1982). DOI doi.org/10.1103/PhysRevD.25.2951
6. A. Strumia and F. Vissani, Nucl. Phys. B **726**, 294 (2005). DOI 10.1016/j.nuclphysb.2005.07.031.
7. O. Azzolini et al., Eur.Phys.J. C **78** no.5, 428 (2018). DOI 10.1140/epjc/s10052-018-5896-8.
8. E. Fiorini, T.O. Niinikoski, Nuclear Instruments and Methods in Physics Research A **224**, 83 (1984).
9. E. E. Haller et al., Neutron Transmutation Doping of Semiconductor Materials, (1984) Springer, Boston, MA.
10. D.R. Artusa, et al., Adv. High Energy Phys. **2015**, 879871 (2015). DOI 10.1155/2015/879871
11. C. Alduino et al., [CUORE Collaboration], Phys. Rev. Lett. **120**(13), 132501 (2018). DOI 10.1103/PhysRevLett.120.132501
12. K. Alfonso, et al., Phys. Rev. Lett. **115**(10), 102502 (2015). DOI 10.1103/PhysRevLett.115.102502
13. C. Alduino et al., [CUORE Collaboration], Eur. Phys. J. C **77** (2017) no.8, 543 DOI 10.1140/epjc/s10052-017-5080-6.
14. G. Wang, et al., arXiv:1504.03612 (2015).
15. G. Wang, et al., arXiv:1504.03599 (2015).
16. D. Artusa, et al., Eur. Phys. J. C **74**(10), 3096 (2014). DOI 10.1140/epjc/s10052-014-3096-8.
17. D. Poda and A. Giuliani, Int. J. Mod. Phys. A **32** no.30, 1743012 (2017). DOI 10.1142/S0217751X17430126.
18. O. Azzolini et al., Phys. Rev. Lett. **120** 232502 (2018). DOI 10.1103/PhysRevLett.120.232502.
19. A. S. Barabash, V. B. Brudanin, and NEMO Collaboration, Phys. Atom. Nuclei **74** 312 (2011). DOI 10.1134/S1063778811020062.
20. R. Arnold et al., arXiv:1806.05553 (2018)
21. J.W. Beeman, et al., Eur. Phys. J. **C75**(12), 591 (2015). DOI 10.1140/epjc/s10052-015-3822-x.
22. C. Arnaboldi, et al., Astropart. Phys. **34**, 344 (2011). DOI 10.1016/j.astropartphys.2010.09.004.
23. J.W. Beeman, et al., JINST **8**, P05021 (2013). DOI 10.1088/1748-0221/8/05/P05021.
24. L. Gironi, et al., JINST **5**, P11007 (2010). DOI 10.1088/1748-0221/5/11/P11007.

25. J.W. Beeman, et al., Eur. Phys. J. **C72**, 2142 (2012). DOI 10.1140/epjc/s10052-012-2142-7.
26. J.W. Beeman, et al., Astropart. Phys. **35**, 813 (2012). DOI 10.1016/j.astropartphys.2012.02.013.
27. J.W. Beeman, et al., Phys. Lett. B **710**, 318 (2012). DOI 10.1016/j.physletb.2012.03.009.
28. L. Cardani, et al., J. Phys. **G41**, 075204 (2014). DOI 10.1088/0954-3899/41/7/075204.
29. E. Armengaud, et al., JINST **10**(05), P05007 (2015). DOI 10.1088/1748-0221/10/05/P05007.
30. L. Berge, et al., JINST **9**, P06004 (2014). DOI 10.1088/1748-0221/9/06/P06004.
31. L. Cardani, et al., JINST **8**, P10002 (2013). DOI 10.1088/1748-0221/8/10/P10002.
32. T.B. Bekker, et al., Astropart. Phys. **72**, 38 (2016). DOI 10.1016/j.astropartphys.2015.06.002.
33. D. R. Artusa et al., Eur. Phys. J. C **76** no.7, 364 (2016). DOI 10.1140/epjc/s10052-016-4223-5.
34. E. Armengaud et al., Eur. Phys. J. C **77** no.11, 785 (2017). DOI 10.1140/epjc/s10052-017-5343-2.
35. G. Buse et al., Nucl. Instrum. Meth. A **891** 87 (2018) DOI 10.1016/j.nima.2018.02.101.
36. D.L. Lincoln, et al., Phys.Rev.Lett. **110**, 012501 (2013). DOI 10.1103/PhysRevLett.110.012501.
37. A. S. Barabash, Int. J. Mod. Phys. A **33** 1843001 (2018). DOI 10.1142/S0217751X18430017.
38. M. Berglund and M.E. Wieser, Pure Appl. Chem **83**, 379 (2011).
39. I. Dafinei *et al.*, J. Cryst. Growth **475** 158 (2017) DOI 10.1016/j.jcrysgro.2017.06.013.
40. S. Pirro, et al., Phys. Atom. Nucl. **69**, 2109 (2006). DOI 10.1134/S1063778806120155.
41. J.W. Beeman, et al., JINST **8**, P07021 (2013). DOI 10.1088/1748-0221/8/07/P07021.
42. C. Arnaboldi, G. Pessina, E. Previtali, IEEE Trans. Nucl. Sci. **50**, 979 (2003). DOI 10.1109/TNS.2003.815346.
43. E. Andreotti et al., Nucl. Instr. Meth. A **664** 161 (2012). DOI 10.1016/j.nima.2011.10.065.
44. C. Arnaboldi et al., Journal of Instrumentation, **13**(02), 02026 (2018). DOI 10.1088/1748-0221/13/02/P02026.
45. P. Carniti et al., Rev. Sci. Instr. **87** 054706 (2016). DOI 10.1063/1.4948390.
46. C. Arnaboldi and G. Pessina, J. Low Temp. Phys. **151** 964 (2008). DOI 10.1007/s10909-008-9785-7.
47. C. Arnaboldi et al., Rev. Sci. Instr. **86** 124703 (2015). DOI 10.1063/1.4936269.
48. C. Arnaboldi et al., Nucl. Instr. Meth. A **617** 327 (2010). DOI 10.1016/j.nima.2009.09.023.
49. S. Pirro, Nucl. Instr. Meth. A **559**, 672 (2006). DOI 10.1016/j.nima.2005.12.197.
50. C. Arnaboldi, G. Pessina, S. Pirro, Nucl. Instrum. Meth. A **559**, 826 (2006). DOI 10.1016/j.nima.2005.12.210.
51. C. Arnaboldi, et al., Nucl. Instrum. Meth. A **520**, 578 (2004). DOI 10.1016/j.nima.2003.11.319.
52. C. Arnaboldi, et al., IEEE Trans. Nucl. Sci. **49**, 2440 (2002).
53. S. Di Domizio, "Search for double beta decay to excited states with CUORICINO and data acquisition system for CUORE", PhD Thesis, Università degli Studi di Genova (2009).
54. S. Copello, "Dark Matter induced annual modulation analysis in CUORE-0", PhD Thesis, Università degli Studi di Genova (2017).
55. C. Alduino et al., [CUORE Collaboration], Phys. Rev. C **93** no.4, 045503 (2016). DOI 10.1103/PhysRevC.93.045503
56. J. L. Ouellet, "The Search for 0ν DBD in Te-130 with CUORE-0", PhD Thesis, University of California, Berkeley (2015).
57. A. D. Bryant, "A Search for Neutrinoless Double Beta Decay of Te-130", PhD Thesis, University of California, Berkeley (2010).
58. J. S. Cushman, "A search for neutrinoless double-beta decay in tellurium-130 with CUORE", PhD Thesis, Yale University (2018).
59. E. Gatti, P.F. Manfredi, Riv. Nuovo Cimento **9**, 1 (1986)
60. V. Radeka, N. Karlovac, Nucl. Instrum. Meth. **52**, 86 (1967)
61. A. Alessandrello et al., Nucl. Instr. Meth. A **412** 454 (1998).
62. K. Alfonso et al., JINST **13** P02029 (2018).
63. N. Casali et al., J. Phys. G: Nucl. Part. Phys. **41** 075101 (2014). DOI 10.1088/0954-3899/41/7/075101
64. O. Azzolini et al., "Analysis of cryogenic calorimeters with light and heat read-out for double beta decay searches," arXiv:1806.02826 (2018).